# Seismic damage assessment of a crude oil hydrodesulphurisation unit. Part I: exposure and modelling

**Carlos Grajales-Ortiz[a,*], Vasileios E. Melissianos[b], Konstantinos Bakalis[b], Mohsen Kohrangi[c], Paolo Bazzurro[a], and Dimitrios Vamvatsikos[b]**

## Abstract

The assets of a hydrodesulphurisation unit of a crude oil refinery are presented in sufficient detail to create a system-wide model for seismic fragility and risk assessment. The assets include pumps, liquid storage tanks, heat exchangers, equipment-supporting buildings, furnaces, process towers, high-temperature separators, and the piping network. Simplified numerical models were employed for the assets, accounting for salient characteristics, functionality, and interconnectivity thereof. Most importantly, a full 3D model of the piping network is provided, which incorporates a simplified representation of the connected structures to capture the dynamic interaction with the piping, enabling cost-effective assessment; increased flexibility in fittings, i.e., elbows, tees, and nozzles, is also accounted for. The end goal is to address the complexities of a small yet critical part of a modern refinery unit and offer a well-documented basis for conducting seismic damage assessment of a critical energy system, which is presented in the companion paper.

## Keywords

Crude oil refinery, hydrodesulphurisation unit, exposure model, piping, process assets

## 1 Introduction

Crude oil refineries play a pivotal role in modern society, serving as the core facilities for processing crude oil into a multitude of refined products, such as gasoline, diesel, jet fuel, and various other petroleum-based products that power transportation, heating, and industrial processes. A crude oil refinery is a complex infrastructure functioning as an integrated system that relies on the smooth and uninterrupted operation of various interconnected components like liquid storage tanks, pumps, process towers, and pressure vessels. However, refineries are vulnerable to natural-technological (NaTech) accidents that may result in severe consequences, spanning from production interruption to fire or explosions. The impacts can be of such magnitude as to be considered credible threats to human health and life, the environment, and the economy (e.g., [1-7]). In particular, earthquake-induced NaTech events have often led to substantial economic and human losses, despite their comparatively lower frequency of occurrence compared to NaTech events caused by storms, tropical storms, extreme temperatures, lightning, or flooding [7].

Accordingly, researchers have developed numerical models for assessing the seismic response of individual industrial structures, such as liquid storage tanks, pipelines, and pressure vessels. The perspectives of these studies vary, with some introducing complex asset-specific and detailed-laden models for pressure vessels (e.g., [8-10]), liquid storage tanks (e.g., [11-12]), piping systems (e.g., [11]), and non-structural components and their supporting structure (e.g., [13]), while others utilising reduced-order models that trade accuracy for generality and

[a] University School for Advanced Studies IUSS Pavia, Pavia, Italy
[b] Institute of Steel Structures, School of Civil Engineering, National Technical University of Athens, Greece
[c] RED Risk Engineering + Development, Pavia, Italy
* Corresponding author: E-mail address: carlos.grajales@iusspavia.it (C. Grajales-Ortiz).

reduced computational cost for pressure vessels (e.g., [14]), liquid storage tanks (e.g., [15-18]), piping systems (e.g., [19, 20]), high-rise stacks (e.g., [21]), and non-structural components with their equipment-supporting buildings (e.g., [22]). Simplified models for pressure vessels have focused on modelling the response of assets such as spherical shells [14] and steel process towers [21]. For liquid storage tanks, early simplified models represented the tanks by constructing an equivalent system comprising an equivalent impulsive fluid mass and an equivalent convective fluid mass [15, 17]. Later models included the uplifting response, which occurs when the base of a tank partially lifts off the ground and influences the overall seismic behaviour of both anchored and unanchored tanks [16, 18]. Simplified models for piping systems have primarily focused on representing the behaviour of pipe segments, with particular emphasis on elbows, which present an increased flexibility compared to straight piping segments and can be more susceptible to seismically induced damage [19, 20]. High-rise stack simplified models include steel chimneys, reinforced concrete chimneys, and steel flares [21]. Modelling of building-type industrial structures include reinforced concrete and steel structures [22]. Non-structural components (i.e., equipment items), such as pumps and heat exchangers, are not explicitly modelled in [22] but included as point masses only in the buildings; their seismic response is evaluated by recording peak component acceleration demands and comparing them to the capacity of each components' anchorage system. In other words, only anchorage failure is captured in this simplified modelling approach.

Particularly for crude oil refineries, there is a substantial body of literature on the numerical models and associated fragility of liquid storage tanks (e.g., [16, 18]), piping systems (e.g., [19, 20]), equipment-supporting buildings (e.g., [22]), and high-rise stacks [21]. However, the aforementioned studies have mostly focused on individual structures, with fewer attempts made to model assets that belong to the same process unit and are functionally and physically interconnected via piping (e.g., [11, 23]). Herein, we aim to provide a comprehensive model of both individual assets and their interconnections via the piping network, enabling a comprehensive representation of a hydrodesulphurisation unit, which lays in the heart of the refining process. In the companion paper [24], this exposure model is used to demonstrate a hazard-consistent (i.e., representative of the hazard of the site) methodology for developing individual asset fragilities and assessing the seismic damage of such critical crude oil refinery units. Ultimately, the detailed exposure model developed in this study is the first step towards performing a comprehensive and advanced seismic risk assessment of a hydrodesulphurisation unit.

## 2 Hydrodesulphurisation Unit Exposure Model

The purpose of a hydrodesulphurisation (HDS) unit in a typical crude oil refinery is to generate a product, such as diesel, with a sulphur content below a specified threshold [25], e.g., 10 parts per million (ppm) as per the EU Directive 2009/30/EC [26] on the specification of petrol, diesel, and gasoil. The individual structurally independent assets under consideration in the HDS unit exposure model are listed in Table 1. It should be noted that this is not an extensive list of all industrial assets present in the HDS process, but only a list of those that play a critical role in the process and, therefore, are considered assets at risk in case of an earthquake. The HDS unit is relatively simple, especially in terms of piping relative to other very complex refinery units, and at the same time it includes a number of diverse refinery assets that offer depth to the modelling discussion. Most importantly, damage to the HDS unit is critical not just at the facility but also for the surrounding populated areas due to the high toxicity of the stored and processed products.

Table 1. Structurally independent assets of HDS unit considered in the analysis.

| Asset description | Asset ID |
|---|---|
| Liquid storage tanks | TK-01, TK-02, TK-03, TK-04 |
| Pumps | P-01, P-01S, P-02, P-02S |
| Heat exchangers | E-01, E-02A, E-02B, E-03A, E-03B |
| Furnace | H-01 |
| Reactors | R-01, R-02 |
| High-temperature separator | V-01 |
| Stripper | C-01 |

The schematic plan of the HDS unit is shown in Figure 1. The raw material processed in the HDS unit is naphtha, which is imported from other upstream refinery units and is stored in two liquid storage tanks (TK-01/02). It is then transported to a series of heat exchangers (E-01, E-02/03A&B), which are nested in an equipment-supporting building; they preheat (i.e., increase the temperature of) the fluid before entering the furnace (H-01). Within the furnace, the fluid undergoes further heating to achieve the requisite processing temperature for the reactors. The hot outlet steam from the furnace is directed to the reactors (R-01/02), where the sulphur content is converted to hydrogen sulphide with the aid of a catalyst. Past the reactors, the fluid passes through two heat exchangers (E-03A&B) for cooling. A high-temperature separator (V-01) then separates the cooled reacted fluid from the hydrogen sulphide. The liquid phase of the desulphurised product is sent to a stripper (C-01), where light fractions are removed with the assistance of steam. Finally, the fluid is transported to a heat exchanger (E-01) for further temperature reduction, before being transported to two liquid storage tanks (TK-03/04). Pumps (P-01/02, P-01S/02S) located within the piping network ensure the circulation of the fluid and its delivery to each unit asset at the necessary pressure.

It should be noted that complex industrial systems, such as petrochemical plant units, usually incorporate redundancies to a certain extent. This means that some of the assets can be set off order, e.g., for regular maintenance or unscheduled repairs, with little or no consequence to the production. Also, some assets can operate simultaneously, adopting a partially-in-parallel configuration for increased productivity of the unit. Specifically, each pump in the HDS unit, P-01 and P-02, has a corresponding spare pump, P-01S and P-02S, respectively, that can completely replace the primary pump without consequences to the unit operation. On the other hand, heat exchangers E-02/03A operate partially-in-parallel with E-02/03B, similarly to how reactors R-01 and R-02, and tanks TK-01 with TK-02 function. Taking any of these partially-in-parallel assets offline will reduce productivity, but operations will not cease.

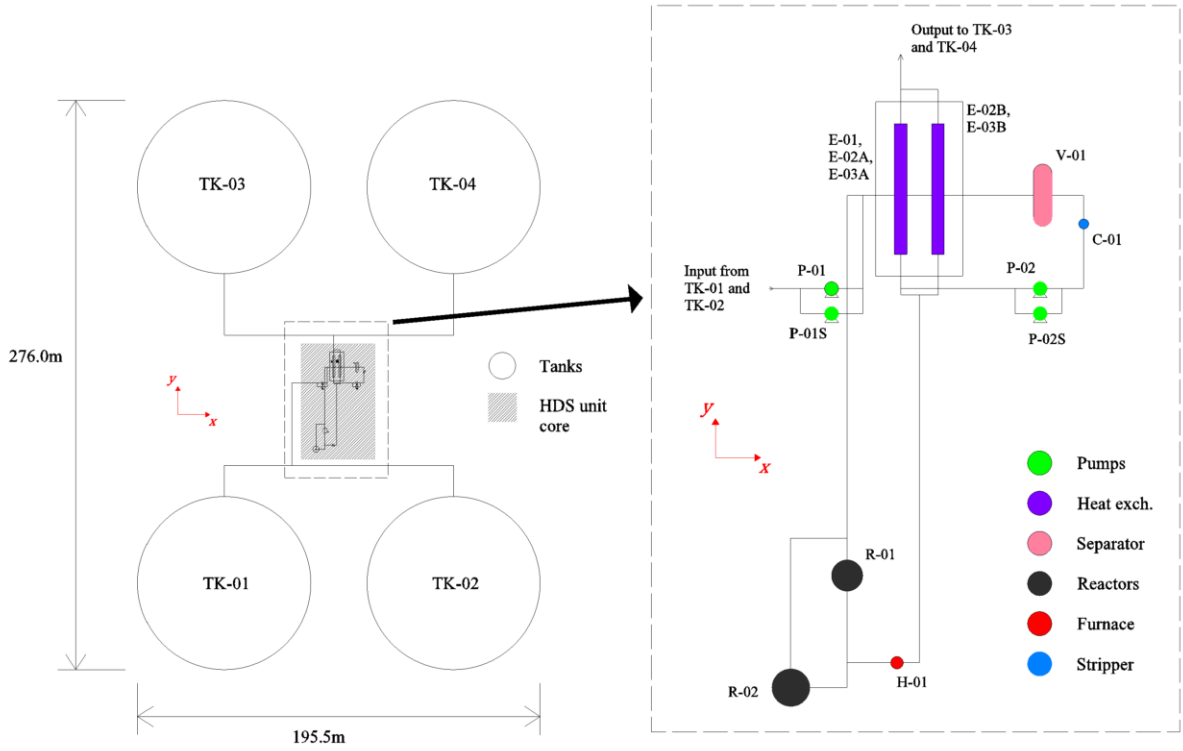


Figure 1. Schematic plan of the entire HDS unit including the liquid storage tanks.

## 3 Asset Structural Models

The assets of the HDS unit are detailed in the subsequent sections, focusing on the mechanical models developed or adopted for their assessment. For ease-of-use and expediency, simplified (reduced-order and surrogate) models are employed, which are suitable for a seismic risk assessment study. They capture only high-level salient characteristics, rather than all details of the structures, in a mode of application consistent with portfolio-level, rather than structure-specific assessment. In all cases, models are strictly structural, neglecting any soil-structure interaction by assuming the presence of firm soil conditions. The OpenSees platform [27] is employed to model the seismic response of all the assets. As reference, it is recalled that standards for (typically non-seismic) design, manufacturing, construction, and operation of industrial assets for crude oil refineries such as pumps, heat exchangers, and pressure vessels include the ASME Boiler and Pressure Vessel Code (BPVC) Section VIII [28], API 610 [29], and API 660 [30]. Finally, it is noted that the examined assets are considered to be corrosion- and defect-free, as well as sufficiently maintained as pre standard industry practice.

### 3.1 Liquid storage tanks

Four atmospheric unanchored liquid storage tanks are considered in the HDS unit. The properties and content of the are listed in Table 2. As discussed in, for example, Bakalis et al. [18] and Karaferis et al. [31], the fill ratio determines the structural response of liquid storage tanks. Indeed, the impulsive fluid component of the tank, which is the part of the contained fluid that moves “rigidly” with the tank walls, and the convective fluid component, which develops a sloshing motion on the free surface due to earthquake excitation, are closely related to the volume of the fluid contained in the tank that is represented by the fill ratio, i.e., fluid height over total tank height. To account for this effect, three characteristic fill ratios are considered, resulting to the development of three distinct tank models per tank type: an almost

full tank with 90% fill ratio, a roughly half-full tank with 60% fill ratio, and a nearly empty tank with 30% fill ratio. The surrogate numerical model developed by Bakalis et al. [18] is adopted here to assess the seismic performance of the liquid storage tanks. The Bakalis et al. [18] tank model is employed for the tanks under investigation, assuming that the latter are unanchored (resting on a concrete foundation) and have a fixed roof. The tank model consists of a single mass, which is representative of the impulsive fluid mass, connected to an elastic beam-column element; the latter is supported by a set of radial rigid-beam spokes, each resting on multilinear elastic edge springs to account for uplifting. Three critical failure modes are considered in the model, namely roof and upper shell damage due to sloshing, excessive base plate rotation, and elephant's foot buckling of the lower shell course. Only sliding is not accounted for. The vibration periods of the impulsive and convective masses of the tanks are listed in Table 3. As a final remark about the tanks, it is acknowledged that, in many cases, volatile liquids are stored in tanks with a floating roof. Still, the tanks of the examined HDS unit are fixed-roof ones.

Table 2. Liquid storage tanks of the HDS unit and their salient characteristics [$\rho_f$: product density, $H_t$: tank height, $R$: tank radius, $t_b$: base plate thickness, $t_a$: annular ring thickness, $t_w$: equivalent wall thickness, $f_y$: steel yield strength].

| ID | Product | $\rho_f$ (kg/m$^3$) | $H_t$ (m) | $R$ (m) | $t_b$ (mm) | $t_a$ (mm) | $t_w$ (mm) | $f_y$ (MPa) |
|---|---|---|---|---|---|---|---|---|
| TK-01/02 | Naphtha | 750 | 22.0 | 42.7 | 6.4 | 11.0 | 33.2 | 235 |
| TK-03 | Gasoline | 750 | 22.0 | 42.7 | 6.4 | 11.0 | 33.2 | 235 |
| TK-04 | Gasoil (Diesel) | 845 | 22.0 | 42.7 | 6.4 | 11.0 | 33.2 | 235 |

Table 3. Vibration periods of fluid components of tanks with different fill ratios [$T_i$: impulsive vibration period, $T_c$: convective vibration period].

| ID | Fill ratio (%) | $T_i$ (s) | $T_c$ (s) |
|---|---|---|---|
| TK-01/02 | 90 | 0.35 | 15.02 |
| | 60 | 0.24 | 13.26 |
| | 30 | 0.11 | 11.50 |
| TK-03 | 90 | 0.35 | 15.02 |
| | 60 | 0.24 | 13.26 |
| | 30 | 0.11 | 11.50 |
| TK-04 | 90 | 0.37 | 15.02 |
| | 60 | 0.26 | 13.26 |
| | 30 | 0.12 | 11.50 |

## 3.2 Pumps

The pumps of the examined HDS unit are all located on the ground level, which is typical practice in refineries. Pumps are a critical part of the refinery units as they ensure the smooth and sufficient (i.e., in correct pressure and flow volume) circulation of fluids in the extensive piping network. Pumps are modelled as single degree of freedom (SDOF) systems and are considered to be anchored to a solid concrete foundation. Each pump weights 500kg. A damping ratio of 2% is adopted based on the suggested values by Kazantzi et al. [22]. The fundamental periods of all the pumps are assumed to be equal to 0.10s in both $x$ and $y$

directions, due to the strong fixed conditions of the machinery on its foundation for operational reasons (vibration). A Peak Component Acceleration (PCA) demand is computed by calculating the ground spectral acceleration, based on the acceleration input (i.e., recorded ground motion), evaluated at each pump fundamental period in both the global $x$ and $y$ directions. The earthquake-resistant design of the anchorage has been performed based on the provisions of EN 1998-1:2004 [32]. This essentially implies that overstrength, rather than ductility, is the main seismic resistance mechanism, practically ensuring an elastic response, which is also required for operational reasons.

### 3.3 Equipment-supporting building and heat exchangers

The heat exchangers in the HDS unit are nested within a two-storey equipment-supporting building. The building is a two-storey reinforced concrete moment-resisting open-frame structure. Excluding the area of cantilevers, the building has floor dimensions of 15.2×8.2m with a story height of 5.5m. Heat exchanger E-01 is located at the ground level, while heat exchangers E-02A and E-02B are located on the first floor, and heat exchangers E-03A and E-03B at the second floor. Each heat exchanger weights 10,000kg. The total mass of the building including the nested heat exchangers, other than E-01 on the ground level, is 611,500kg. The equipment-supporting building is considered fixed to the ground and it is depicted in Figure 2. Equipment-supporting industrial buildings are typically of high-strength low-ductility design for non-seismic related reasons, such as operational integrity and fireproofing [22]; therefore, all structural elements of the building are modelled as elastic beam-column elements. The slab at each floor level is modelled as a rigid diaphragm, which implies that the floor slabs are thick enough to provide sufficient in-plane rigidity. Rayleigh damping is employed and in particular a damping ratio of 5% is assigned to the first and second global translational modes of vibration. The first and second modes of vibration of the building, which are 0.21s and 0.20s along the $x$ and $y$ directions, respectively, are shown in Figure 3. The interested reader may find more details about the modelling background in the work of Kazantzi et al. [22].

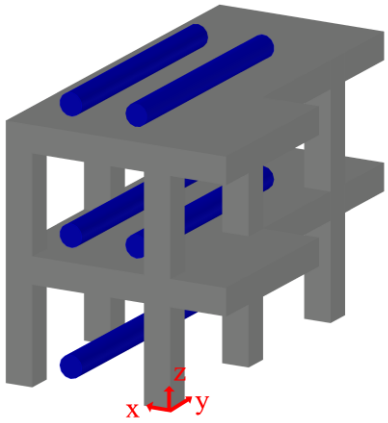


Figure 2. 3D representation of the two-storey equipment-supporting building with its nested heat exchangers shown in blue.

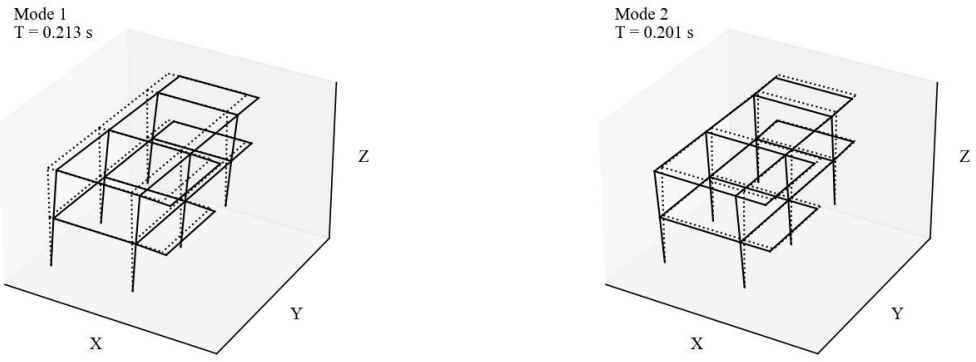


(a) (b)

Figure 3. Vibration modes of the equipment-supporting building: (a) Mode 1 and (b) Mode 2 [the dotted lines represent the undeformed shape, and the solid lines represent the deformed shape].

Heat exchangers on the first and second floor are anchored to the building slab. They are not incorporated explicitly in the building model; instead, the cascade modelling approach is employed, introducing them as point masses in the overall model. This is because their mass of 10,000kg each is significantly lower than the structure's mass; therefore, the effect of dynamic interaction between the structure and components is insignificant (e.g., [33]). For computing heat exchanger response, we use the acceleration time histories at the anchor points of heat exchangers located on floor levels other than the ground. Based on the acceleration input and the estimated period of the heat exchangers in each principal direction, a PCA demand is computed by calculating the corresponding floor spectral acceleration. A damping ratio of 2% is adopted for all heat exchangers. The fundamental periods of all heat exchangers are assumed equal to 0.15s and 0.40s in the global $x$ and $y$ directions, respectively. For the heat exchanger located at the ground level, which is anchored to the building foundation, PCA demand is identical to the ground spectral acceleration evaluated at the component period in the $x$ and $y$ directions, in the same manner as for the pumps. An elastic anchorage system designed as per EN 1998-1:2004 [32] is assumed for the heat exchangers.

### 3.4 Furnace

The furnace in the HDS unit heats the process fluid to the optimal temperature required for the removal of sulphur compounds in the reactors. The compartments of a typical industrial furnace, starting from the lower to the higher level, are the firebox, the radiant section, the convection section, and the stack. In the firebox, which is located at the bottom of the radiant section, burners are placed on the floor or the walls of the shell and produce heat by combustion. The process fluid inside the furnace circulates in tubes. The fluid enters the furnace near the stack (i.e., on the upper part of the shell) and exits the furnace near the bottom, close to the burners. The area closer to the stack is called the convection section because in this area heat transfer is performed primarily through convection, while in the lower area of the shell, heat transfer is primarily performed through radiation, hence the name of the radiant section. The firebox is usually lined internally with a refractory layer, a brick lining specially designed to withstand and reflect heat, while the convection and radiant sections are usually lined with special insulation and refractory materials [34]. Combustion gases that are generated for heat production rise to the stack and are released into the atmosphere.

The examined furnace, being illustrated in Figure 4(a), is a typical cabin furnace used in the petrochemical industry (e.g., [35]). The dimensions of the furnace are listed in Table 4, where width coincides with $x$ axis and length with $y$ axis. The furnace has a total mass of 19,107kg

and is made of S275R steel grade with a mean yield stress of 397.56MPa [36]. The reduced-order numerical model for the analysis of the furnace is based on the lumped mass model shown in Figure 4(b) and the guidelines of Karaferis et al. [21]. The developed numerical model consists of concentrated masses attached to elastic beam-column elements. A total of 22 concentrated masses are included. The masses considered represent the self-weight of each segment (i.e., radiant section, convection section, stack transition, stack), also accounting for the firebricks at the bottom of the furnace, the ceramic fibre lining, and internal piping. P-Δ effects are accounted for in the structural analysis. The furnace is anchored (fixed) directly on its concrete mat foundation. It should be noted that in some cases, industrial furnaces are placed on reinforced concrete short columns that can modify the dynamic behaviour due to the presence of weak shear elements. If that were the case, an update of the numerical model would be needed. A damping ratio is set at 2% for both the first and third translation modes of vibration. The modal analysis yielded the fundamental translational period of vibration of the furnace of 0.12s in the global *x* direction and 0.11s in the global *y* direction, with the third mode having a period of 0.03s. Given the adoption of a lumped mass model attached to beam-column elements, no vibration modes are displayed for the furnace. It is noted that non-structural elements, such as internal piping or fibre lining, are not included in the model itself. Instead, the integrity of these elements is indirectly evaluated through appropriate damage states [24].

Table 4. Dimensions of the furnace.

| Furnace section | Parameter | Value |
|---|---|---|
| Stack | Diameter (m) | 0.84 |
| | Height (m) | 9.35 |
| | Shell thickness (mm) | 6.35 |
| Stack transition | Width (m) | 0.94 |
| | Length (m) | 3.30-0.97 |
| | Height (m) | 1.63 |
| | Shell thickness (mm) | 6.35 |
| Convection section | Width (m) | 1.12 |
| | Length (m) | 6.50 |
| | Height (m) | 2.27 |
| | Shell thickness (mm) | 6.35 |
| Radiant section | Width (m) | 2.28 |
| | Length (m) | 6.50 |
| | Height (m) | 4.13 |
| | Shell thickness (mm) | 6.35 |

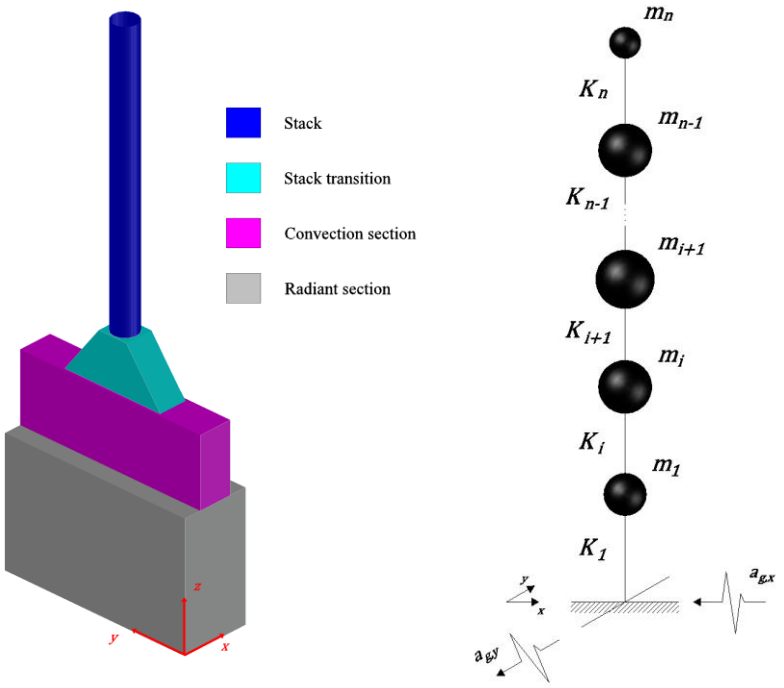


(a) (b)

Figure 4. (a) 3D representation of the furnace; (b) Generic representation of the lumped mass numerical model used for the assessment of the furnace and steel process towers.

### 3.5 Reactors and Stripper

The reactors and the stripper are both steel process towers. Reactors in the HDS unit facilitate chemical reactions under controlled pressure and temperature to remove sulphur compounds from the process fluid. The stripper, on the other hand, separates light hydrocarbons and other volatile components from the process fluid using steam to ensure the final product meets purity specifications. The towers are 32.73m high, with an internal diameter equal to 2.6m. The shell thickness of the towers varies along the height of the structures, resulting in four courses with wall thicknesses equal to 16mm (from 0.00 to 14.85m), 18mm (from 14.85 to 23.65m), 19mm (from 23.65 to 26.83mm), and 18mm (from 26.83 to 32.73m) from base to top. The towers are constructed from S275 grade steel with mean yield strength of 380MPa. The total mass of each tower is 49,000kg. The reactors and the stripper are anchored (fixed) on their concrete mat foundation. As in [9, 21], the base anchorage and skirt support of all the towers are assumed to be sufficiently overdesigned as per standard practice. Therefore, they are assumed not to be vulnerable to seismic action; consequently, uplift, overturning, sliding, or deformations of the skirt shell are not considered in the simplified model. The lumped mass numerical model shown in Figure 4(b) is adopted for the analysis of the process towers. The model consists of 16 concentrated masses connected to elastic beam-column elements. The assigned masses are representative of the structure's self-weight, which varies with varying thickness of different courses along the height of the structure. The stiffness of the beam-column elements is calibrated to represent the stiffness of each tower course. P-Δ effects are accounted for in the structural analysis. A damping ratio of 2% is adopted for the first and third vibration modes. The modal analysis yielded the first and second translational periods of vibration of 0.49s, with a third translational mode of 0.08s. More details on the modelling background can be found in Karaferis et al. [21].

### 3.6 High-temperature Separator

The high-temperature separator is a horizontal vessel that weighs 10,000kg and is located at the ground level. It separates the hydrogen sulphide from the hydrocarbon liquid after the reactor, ensuring efficient recycling of hydrogen and preparing the liquid for further processing. The high-temperature separator, similarly to the pumps and the E-01 heat exchanger, is anchored to the ground via an elastic anchorage system designed as per EN 1998-1:2004 [31]. The separator is modelled as an SDOF system. A damping ratio of 2% is adopted for the separator, with its fundamental periods assumed to be equal to 0.15s and 0.40s in the $x$ and $y$ directions, respectively, based on the values suggested by Kazantzi et al. [22]. The PCA demand is computed by calculating the ground spectral acceleration evaluated at each fundamental period in both the global $x$ and $y$ directions.

### 3.7 Piping

The piping network considered for the HDS unit includes pipes of 6", 10", 12", and 24" (inch) diameter in straight segments, elbows, and tees. The piping network within the HDS unit is above ground without any pipe racks in the unit. Pipe racks are versatile open-frame steel structures that are typically encountered in oil refineries for supporting piping (see, for example, [37]). The refinery unit at hand does not include any pipe racks due to its configuration and arranging of its components/assets. The developed model of the unit includes the main piping that connects the units' main components/assets, while secondary piping has been excluded from the analysis for simplicity reasons. All pipelines are made of API5L-X65 steel grade with a mean yield stress of 448.5MPa. The geometric characteristics of the pipes are shown in Table 5. The diameter-to-thickness ratio ($d_m/t$) is also listed in Table 5 because it determines the slenderness of the pipe and, consequently, characterises its structural response.

Table 5. Geometric characteristics of selected pipes for HDS unit [$d_{out}$: pipe outside diameter, $d_{in}$: pipe internal diameter, $t$: pipe wall thickness, $d_m$: pipe mean diameter].

| Parameter / Pipe diameter (in) | 6" | 10" | 12" | 24" |
|---|---|---|---|---|
| $d_{out}$ (mm) | 168 | 273 | 324 | 610 |
| $d_{in}$ (mm) | 146 | 248 | 299 | 584 |
| $t$ (mm) | 11.0 | 12.5 | 12.5 | 13.0 |
| $d_m$ (mm) | 157 | 261 | 312 | 597 |
| $d_m/t$ | 14.3 | 20.5 | 24.5 | 46.3 |

Elbows, tee junctions, and nozzles (collectively referred to as fittings) were identified as critical locations in the piping network due to their increased flexibility compared to straight pipes and the possible intensification of stresses due to their geometric irregularity [11,19]. Typically, fittings are modelled with shell elements to account for the cross-section ovalisation, local buckling occurrence, and the effect of internal pressure. However, this modelling approach requires results from experimental testing for calibration and may add significant computational cost, particularly for large and/or complex models (e.g., [11, 38-42]).

Particularly for elbows, to overcome the aforementioned limitations, researchers, such as Bursi et al. [19], have accounted for the increment in flexibility by defining an equivalent straight

beam element adjusted to the relevant curved elbow according to EN 13480-3:2017 [43]. Paolacci et al. [40] have carried out a comparative study and showed that there is sufficient convergence between the numerical results obtained from detailed models compared to those from the modified beam elements. To that effect, the latter approach was adopted hereinafter for modelling elbows.

The length of the equivalent straight beam element $L$ is equal to two times the mean diameter of the pipe ($d_m$), following the findings of Bursi et al. [19]. The effect of flexibility of an elbow spreads across this length $L$. An overview of the adopted equivalent straight elbow is offered in Figure 5.

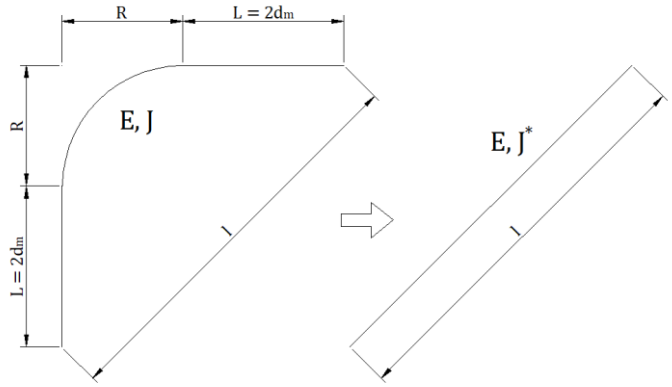


Figure 5. Equivalent straight elbow (adapted from Bursi et al. [19]).

For defining an equivalent straight beam element, an equivalent inertia modulus [19] is estimated as:

$$J^* = \frac{\sqrt{2}J(2d_{out} + R)}{4d_{out} + Rk_B} \tag{1}$$

where $k_B$ is the flexibility factor, defined as the flexibility of an elbow divided by the flexibility of a straight pipe with the same dimensions, $J$ is the inertia modulus of the circular piping section, $d_{out}$ is the elbow outside diameter, and $R$ is the elbow radius. Then, $k_B$ can be calculated after ASME B31.3 [44] as:

$$k_B = \frac{1.65}{h} \tag{2}$$

where $h$ is the flexibility characteristic:

$$h = \frac{4Rt}{d_m^2} \tag{3}$$

while $t$ is the elbow wall thickness and $d_m$ is the elbow mean diameter.

Then, the thickness of the equivalent straight elbow, $t_{eq}$, is calculated from the equivalent inertia modulus as follows:

$$J^* = \frac{\pi}{64}\left(d_{out}^4 - \left(d_{out}^4 - 2t_{eq}\right)\right) \tag{4}$$

It should be noted that the calculation of the parameter $k_B$ after ASME B31.3 leads to over-conservative results [19, 20, 45], a condition that is not desirable for an unbiased assessment of a piping network. Because of this, several researchers (e.g., [19, 45-47]) have developed

numerical models to obtain more realistic flexibility estimates to represent pipe elbows. Figure 6(a) provides examples of these results. This figure illustrates the relationship between $k_B$ and $h$ derived from ASME B31.3, plotted against numerical data from Thomas [45] using the finite difference method, from Martinez et al. [46] using the boundary element method, and from Bursi et al. [19] using the finite element method.

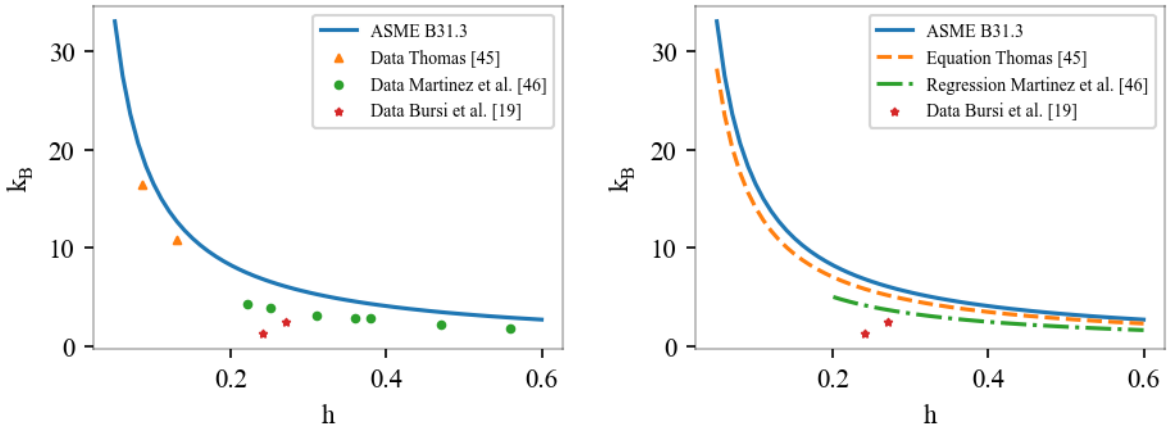


(a) (b)

Figure 6. (a) Flexibility factor $k_B$ as a function of flexibility characteristic $h$ for pipes of varying geometries (i.e., diameter and thickness) using alternative approaches; (b) Flexibility factors $k_B$ for pipes of varying geometries, showing the expressions fitted to Martinez et al. [46], and Thomas [45] against the respective data.

It is observed in Figure 6(a) that the equation given in ASME B31.3 yields larger $k_B$ values for pipes of any given flexibility characteristic $h$, while numerical data produced by Thomas [45], Martinez et al. [46], and Bursi et al. [19] show lower $k_B$ values for the respective pipe geometries analysed.

Based on the data in Figure 6(a), we adopted the following $k_B$ values for our analysis:

- For $h$ values lower than 0.2, the data from Thomas [45] were used because they were the only data points available for this range of $h$. Numerical simulations by Thomas [45] showed that the attached pipe provides a decrease in flexibility of 14.5% compared to the flexibility specified in ASME B31.3, and therefore:

$$k_{B,Thomas} = \frac{1.41}{h} \tag{5}$$

- For $h$ values greater than or equal to 0.2, the data from Martinez et al. [46] were used because they follow a trend similar to that of the ASME B31.3 and the numerical data produced by Thomas [45] but are also closer to numerical data from Bursi et al. [19]. For using the data, we decided to develop a regression model, as plotted in Figure 6(b). The regression equation based on the data from Martinez et al. [46] is:

$$k_{B,Martinez} = \frac{1.01}{h} \tag{6}$$

Note that for more detailed applications, one should ideally develop case-specific numerical models to obtain the values of parameter $k_B$ for the fittings at hand. Nevertheless, the simpler approach adopted fits better our need to efficiently model a refinery unit and offer a scalable methodology that can cover the entire facility as needed. The parameters of the equivalent elbows for the piping network of the HDS unit are tabulated in Table 6.

Table 6. Parameters for equivalent elbows [$d_{out}$: pipe outside diameter, $d_{in}$: pipe internal diameter, $t$: pipe wall thickness, $d_m$: pipe mean diameter, $R$: elbow radius, $h$: elbow flexibility characteristic, $k_B$: elbow flexibility factor, $J$: pipe inertia modulus, $J^*$: inertia modulus of equivalent straight pipe, $t_{eq}$: wall thickness of the equivalent straight pipe].

| Parameter / Pipe diameter (in) | 6” | 10” | 12” | 24” |
|---|---|---|---|---|
| $d_{out}$ (mm) | 168 | 273 | 324 | 610 |
| $d_{in}$ (mm) | 146 | 248 | 299 | 584 |
| $t$ (mm) | 11.0 | 12.5 | 12.5 | 13.0 |
| $d_m$ (mm) | 157 | 261 | 312 | 597 |
| $d_m/t$ | 14.3 | 20.5 | 24.5 | 46.3 |
| $R$ (mm) | 252 | 410 | 486 | 915 |
| $h$ | 0.45 | 0.30 | 0.25 | 0.13 |
| $k_B$ (Adopted) | 2.25 | 3.35 | 4.03 | 10.56 |
| $k_B$ (ASME B31.3) | 3.67 | 5.47 | 6.59 | 12.36 |
| $J$ (mm4) | 1.68E+07 | 8.70E+07 | 1.49E+08 | 1.09E+09 |
| $J^*$ (mm4) | 1.13E+07 | 4.77E+07 | 7.32E+07 | 2.71E+08 |
| $t_{eq}$ (mm) | 6.9 | 6.4 | 5.8 | 3.1 |
| $d_{out}$, elbow (mm) | 168 | 273 | 324 | 610 |
| $d_{in}$, elbow (mm) | 161 | 267 | 318 | 607 |

Tee junctions and nozzles have also been identified as critical locations that may compromise the integrity of piping systems. Detailed numerical models using shell elements have been developed by researchers to represent the experimental behaviour of tee junctions and nozzles (e.g., [11]). Nevertheless, research involving simplified or equivalent beam elements for fittings has been focused mostly on elbows and is relatively scarce for tee junctions and nozzles. ASME B31.3, for example, recommends a flexibility factor $k_B$ equal to 1.0 for tee junctions, and does not give any recommendation for nozzles. Because of this scarcity of data, the elbow parameters in Table 6 have also been adopted for tees and nozzles.

Specifically, for tees, we assume a distance $L = 2d_m$ from the tee intersection point for stiffness reduction, with $d_m$ being the mean diameter of the pipe, as shown in Figure 7(a). This distance $L$ is the same that Bursi et al. [19] adopted to account for the spreading of flexibility from an elbow into the connected straight pipe. For nozzles, the same distance $L$ for the stiffness reduction is assumed, with distance $L$ being measured from the intersection of the piping with each component, as shown in Figure 7(b). It is noted that this length $L$ is adopted due to a lack of data in the literature. Again, a more detailed application should include customised numerical models for obtaining a more accurate representation of $L$ and $k_B$, but this refinement is out of the scope of our study.

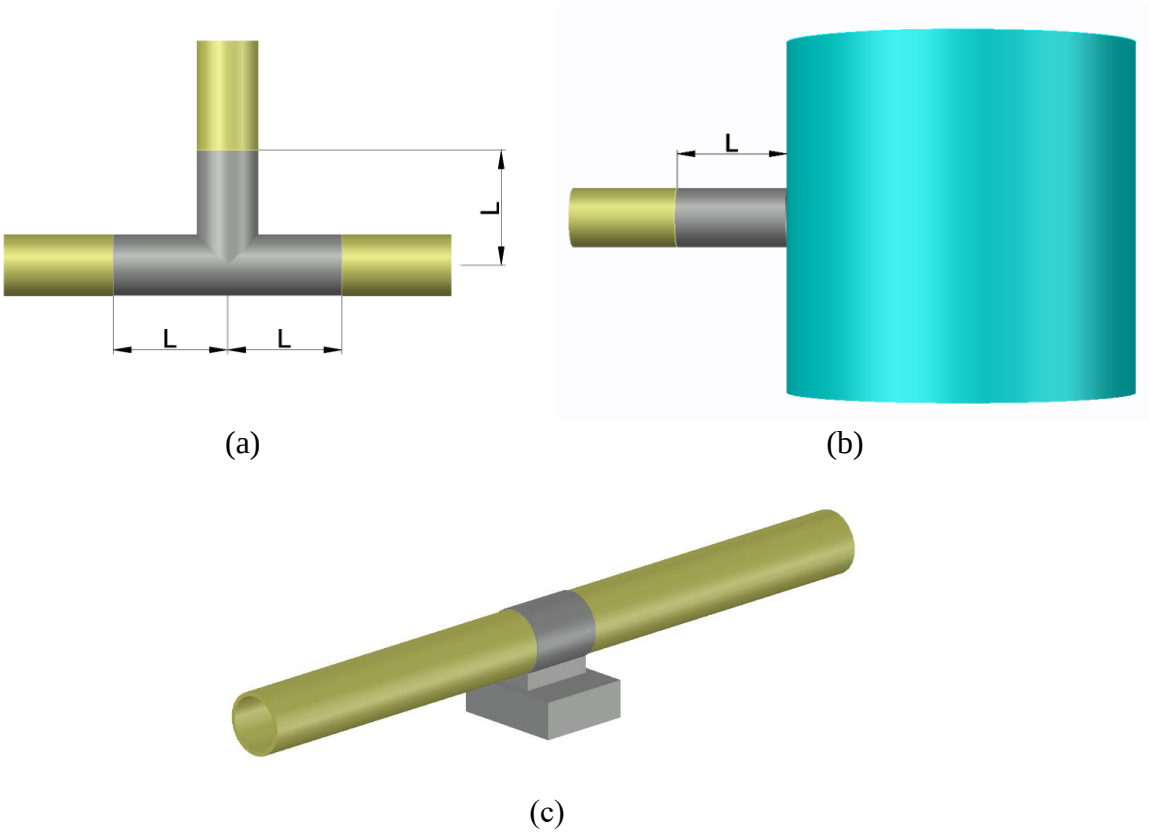


Figure 7. (a) Distance for stiffness reduction in tees; (b) Distance for stiffness reduction in nozzles; (c) Pipe resting on concrete sleeper.

Regarding supports, the piping in consideration rests on concrete bases, so-called "sleepers", as depicted in Figure 7(c). Sleepers are placed every 5m in straight segments and additionally at locations where elbows or tees are present, as per industry practice. Sleepers provide full restraint in the vertical direction, no restraint in the longitudinal direction, and partial restraint in the transverse direction. A maximum allowable lateral displacement equal to 50% of the pipe outer diameter is assumed in the transverse direction following typical construction practice in order to allow small transverse displacement due to thermal expansion. To model this behaviour, we employed the so-called "gap" material available in the OpenSees library to introduce a zero-length composite transverse spring connecting the pipe to the sleeper that allows a zero-stiffness translation in both tension and compression response before engaging a stiff resistance.

To preserve the interaction of piping with the connected assets, such as liquid storage tanks, the dynamic characteristics of said assets should be introduced in the piping network model. The model of the equipment-supporting building is incorporated in its full extent, to ensure capturing the differential displacement of pipes connecting equipment at different floors. Ideally, this would also be done for all assets, leading to a comprehensive piping-and-asset HDS unit model. Given that little information is available about the piping connections to these assets and to lighten the computational load, all non-building assets are replaced by a two-degree-of-freedom single-mass approximation. Specifically, concentrated masses are introduced at the interconnection locations, with translational mass values that match the total asset mass. Elastic translational zero-length springs are attached to said masses in each global direction ($x$ and $y$). They are calibrated so that the period in each direction coincides with the respective fundamental period of the corresponding asset. Thus, they preserve the fundamental modes of the assets, only missing some higher mode effects. Note that, per the employed

approximation, all piping is assumed to be connected to the asset at the effective first-mode height. In reality, different pipes may be connected at different heights, requiring some detailed information (that is not always available) and a somewhat more complex model to account for the dependence of deformation response on the attachment height. For simplicity, we opted for the height-independent approach. It is noted that, as the piping system model depends on the translational mass and fundamental period of each interconnected asset (e.g., tanks or reactors), it also depends on the liquid storage tanks fill ratio that the defines the vibrating mass of the tank. Following a sensitivity analysis, it was found that the structural response of the piping model is not significantly affected by variations in tank fill ratios. Therefore, it was decided to select a set of predefined characteristic fill ratios for the tanks, namely TK-01, TK-02, and TK-04 with a 60% fill ratio and TK-03 with 90% fill ratio to represent the typical operational condition of the HDS unit. It is noted that the effect of the pipe on each single asset is not considered, but, contrarily, the effect of each single asset on the pipe system is taken into account. In other words, aspects such as pipe-to-tank connections (e.g., nozzles) and integrity of piping mechanical components (e.g., valves) are not examined because their impact on the seismic risk is nontrivial and requires detailed further investigation.

Straight piping segments are modelled with elastic beam elements, while elbows, tees, and nozzles are modelled with distributed-plasticity elements based on the force formulation. The Ramberg-Osgood [48] stress-strain relationship is adopted to account for the material nonlinearity in elbows, tees, and nozzles. The material parameters for API5L-X65 steel grade are adopted from Kouretzis et al. [49]. P-Δ effects are accounted for the entire piping model.

The piping network connecting all internal components of the HDS unit is depicted in Figure 8, and the full piping network, including the liquid storage tanks, is depicted in Figure 9. In both figures assets are represented by dots and piping segments are represented by straight lines. The damping ratio for all piping elements is set equal to 0.5% in the first and second modes of vibration based on the suggestions from Bursi et al. [19]. The fundamental period of vibration of the piping system is equal to 8.7s, while the second and third periods of vibration are 7.4s and 6.4s, respectively. The vibration modes of the piping system are displayed in Figure 10. Given that different parts of the piping system are excited in different vibration modes, the first 6 vibration modes of the system are plotted to offer an overview of the piping response. Also, to showcase these different parts of the piping system, the full system for modes 1 to 3 [Figure 10(a) to Figure 10(c)] and only the central part of the system for modes 4 to 6 [Figure 10(d) to Figure 10(f)] are plotted.

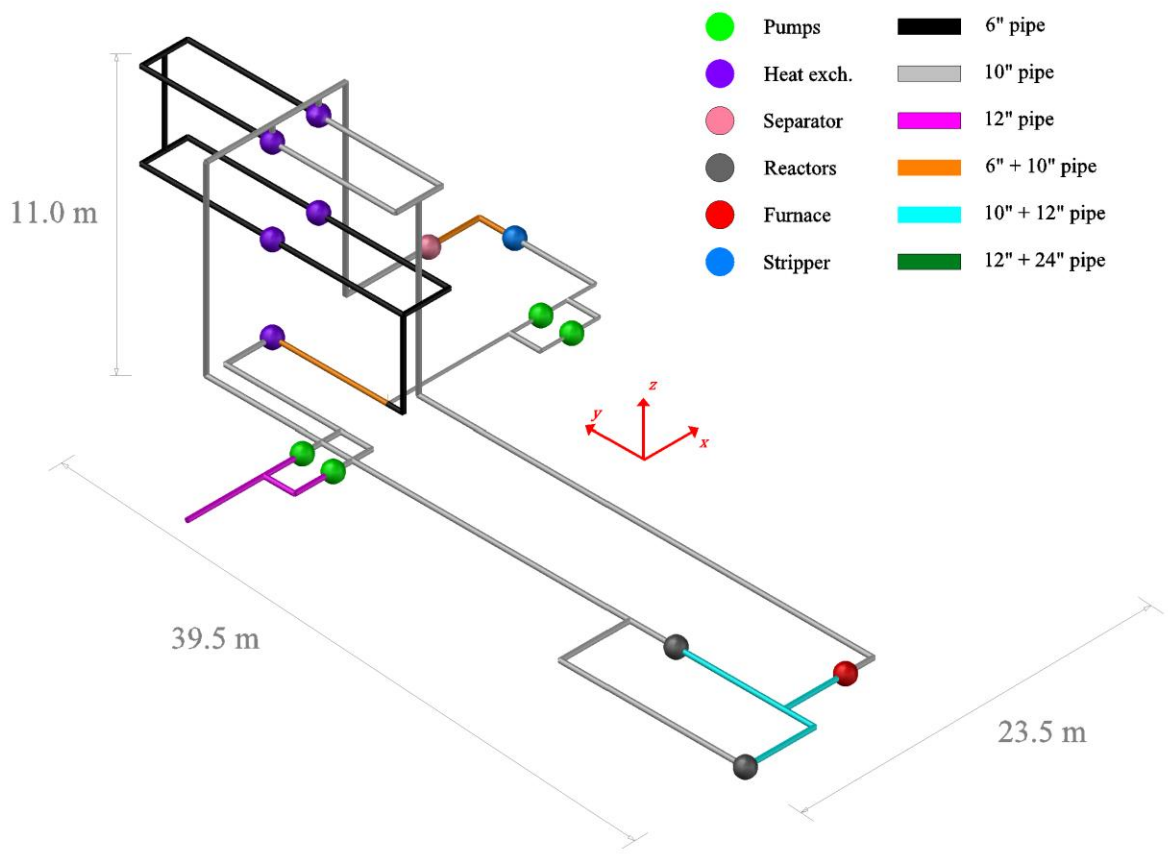


449

450 Figure 8. Piping network connecting components of the HDS unit.

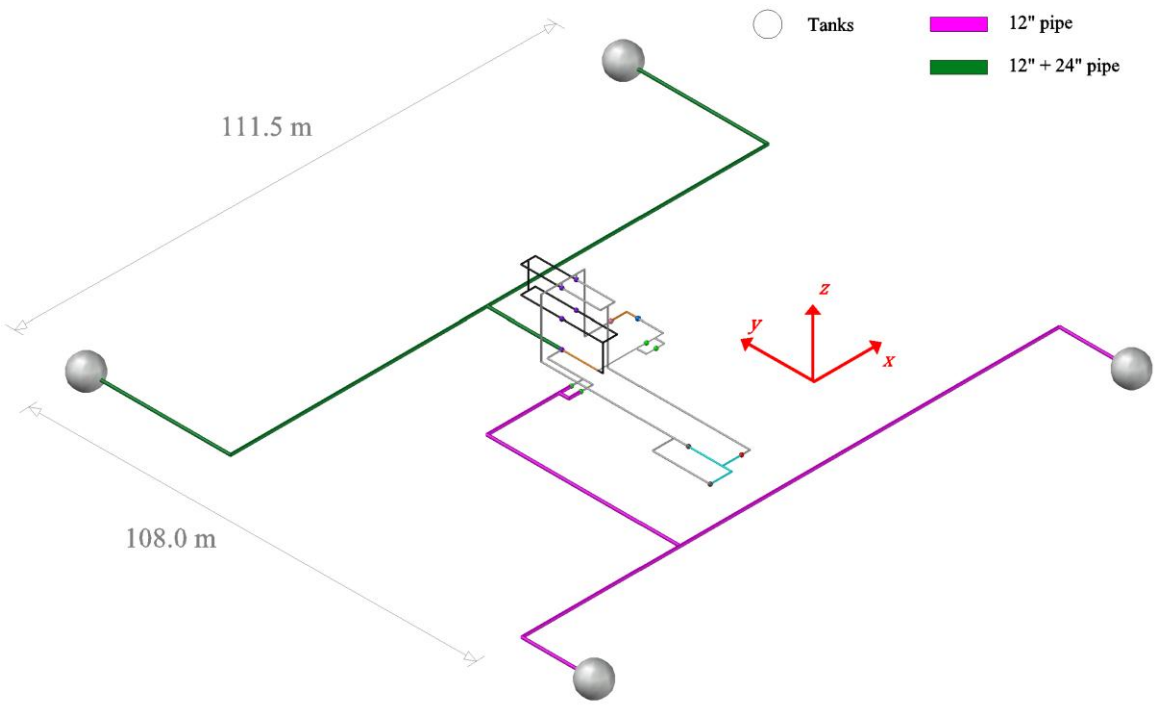


451

452 Figure 9. Piping network connecting assets of the HDS unit, appearing in detail in Figure 8, with the
453 four liquid storage tanks.

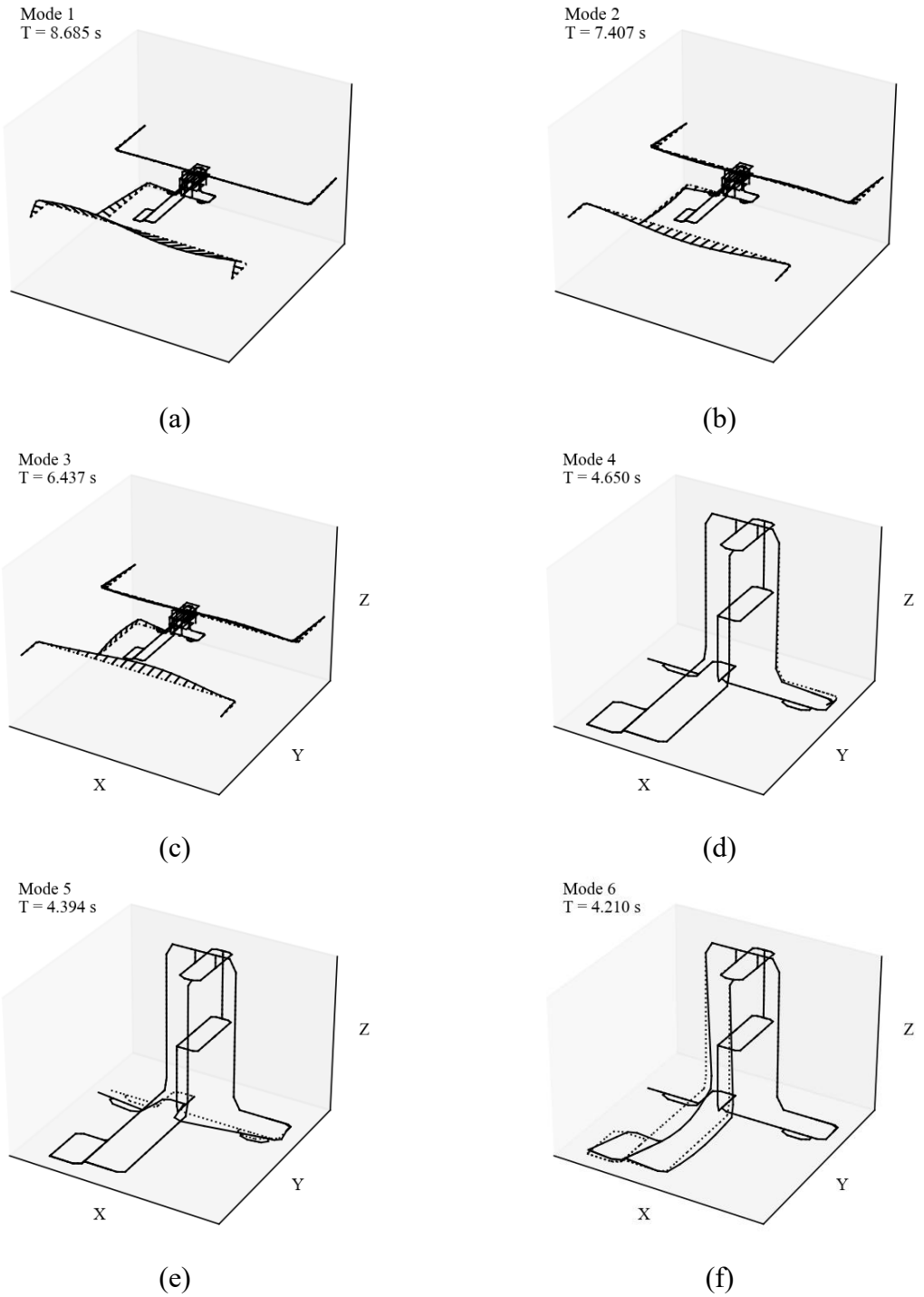


Figure 10. Vibration modes of the piping system: (a) Mode 1; (b) Mode 2; (c) Mode 3; (d) Mode 4; (e) Mode 5; (f) Mode 6. Plots (a) to (c) show the entire piping system, and plots (d) to (f) show the central part of the piping system. The dotted lines correspond to the undeformed shape, while the solid ones to the deformed shape.

## 4 Conclusions

The make-up, operation, and modelling of the critical assets in a hydrodesulphurisation unit of a typical crude oil refinery were presented: liquid storage tanks, pumps, heat exchangers, an equipment-supporting building, a furnace, reactors, a high temperature separator, a stripper, and the connecting piping network. Reduced-order numerical models were developed for the unit assets, while an available surrogate model for the liquid storage tanks was adopted from

the literature. In order to account for the operational and (partial) structural interconnection of the assets via piping, a novel reduced-order model of the piping network was developed considering in detail its critical parts, namely tees and elbows (fittings), together with the salient dynamic characteristics of the assets. Modelling this dynamic interaction of assets and piping is critical for the piping, but also for the functionality of the unit, as even a single pipe failure can have significant operational and safety consequences. Therefore, including such interactions in the piping model is essential to offer high-fidelity risk estimates. The reduced-order models typically offer a simplified representation of the actual assets. Still, they do capture the main functional and structural failure modes necessary for seismic fragility and risk assessments. Far from typical building-stock urban or regional exposure studies, the ensemble of these assets is much more than just a sum of the respective parts. This is a cohesive production unit, whose operation depends on the individual assets in a complex way, allowing for redundancies in some cases (e.g., pumps and reactors), but not in others (e.g., stripper, separator, furnace). The developed exposure model and the numerical models of the interconnected assets presented are then employed for the seismic damage assessment of the refinery critical unit in the companion paper [24].


## Acknowledgements

The first author would like to sincerely thank EUCENTRE and IUSS Pavia for the funding provided. Additional funding was provided by the European Union under Horizon-Europe project PLOTO (Grant Agreement No. 101069941). Also, the authors would like to thank Prof. Denis Sarigiannis and Mr. Achilleas Karakoltzidis (Aristotle University of Thessaloniki) for their help in developing the case study and understanding the HDS operation, as well as Dr. Nikolaos D. Karaferis (National Technical University of Athens) and Prof. Athanasia K. Kazantzi (International Hellenic University) for their valuable support on the development of some of the numerical models used in the study.


## Declaration of conflicting interests

The authors declare no potential conflicting interests concerning the research, authorship, and/or publication of this article.


## ORCID IDS

Carlos Grajales-Ortiz https://orcid.org/0009-0002-4029-0850

Vasileios E. Melissianos https://orcid.org/0000-0002-1589-0697

Konstantinos Bakalis https://orcid.org/0000-0002-0826-1059

Mohsen Kohrangi https://orcid.org/0000-0001-9151-0361

Paolo Bazzurro https://orcid.org/0000-0001-6107-9451

Dimitrios Vamvatsikos https://orcid.org/0000-0002-4016-5040


## References

[1] L. J. Steinberg and A. M. Cruz, When natural and technological disasters collide: Lessons from the Turkey earthquake of August 17, 1999. Natural Hazards Review 5 (3) (2004) 121–130, https://doi.org/10.1061/(ASCE)1527-6988(2004)5:3(121)

[2] S. Young, L. Balluz, and J. Malilay, Natural and technologic hazardous material releases during and after natural disasters: A review. Science of The Total Environment 322 (1–3) (2004) 3–20, https://doi.org/10.1016/S0048-9697(03)00446-7

[3] M. Campedel, Analysis of major industrial accidents triggered by natural events reported in the principal available chemical accident databases. EUR 23391 EN. JRC42281, Publications Office of the European Union, Luxembourg (2008). https://publications.jrc.ec.europa.eu/repository/handle/JRC42281

[4] E. Krausmann, V. Cozzani, E. Salzano, and E. Renni, Industrial accidents triggered by natural hazards: An emerging risk issue. Natural Hazards and Earth System Science 11 (3) (2011) 921–929, https://doi.org/10.5194/nhess-11-921-2011

[5] E. Krausmann, E. Renni, M. Campedel, and V. Cozzani, Industrial accidents triggered by earthquakes, floods and lightning: Lessons learned from a database analysis. Natural Hazards 59 (1) (2011) 285–300, https://doi.org/10.1007/s11069-011-9754-3

[6] H. Nishi, Damage on Hazardous Materials Facilities. International Symposium on Engineering Lessons Learned from the 2011 Great East Japan Earthquake, Tokyo (2012). https://www.jaee.gr.jp/event/seminar2012/eqsympo/pdf/papers/53.pdf

[7] F. Ricci, V. Casson Moreno, and V. Cozzani, A comprehensive analysis of the occurrence of Natech events in the process industry. Process Safety and Environmental Protection 147 (2021) 703–713, https://doi.org/10.1016/j.psep.2020.12.031

[8] A. Di Carluccio, G. Fabbrocino, E. Salzano, and G. Manfredi, Analysis of pressurized horizontal vessels under seismic excitation. 14th World Conference on Earthquake Engineering, Beijing (2008).

[9] H. Moharrami and M. A. Amini, Seismic vulnerability assessment of process towers using fragility curves. Structural Design of Tall and Special Buildings 23(8) (2014) 593–603, https://doi.org/10.1002/tal.1067

[10] I. F. Moschonas, C. Karakostas, V. Lekidis, and Papadopoulos Savvas, Investigation of seismic vulnerability of industrial pressure vessels. 2nd European Conference on Earthquake Engineering and Seismology (2ECEES), Istanbul (2014), https://www.eaee.org/Media/Default/2ECCES/2ecces_ss/2324.pdf

[11] M. Vathi, S. A. Karamanos, I. A. Kapogiannis, and K. V. Spiliopoulos, Performance criteria for liquid storage tanks and piping systems subjected to seismic loading. Journal of Pressure Vessel Technology, Transactions of the ASME 139 (5) (2017) 051801, https://doi.org/10.1115/1.4036916

[12] A. Fiore, C. Rago, I. Vanzi, R. Greco, and B. Briseghella, Seismic behavior of a low-rise horizontal cylindrical tank. International Journal of Advanced Structural Engineering 10 (2) (2018) 143–152, https://doi.org/10.1007/s40091-018-0188-y

[13] G. Quinci, C. Nardin, F. Paolacci, and O. S. Bursi, Modelling of non-structural components of an industrial multi-storey frame for seismic risk assessment. Bulletin of Earthquake Engineering 21 (13) (2023) 6065–6089, https://doi.org/10.1007/s10518-023-01753-4

[14] C. Z. Karakostas, I. F. Moschonas, V. A. Lekidis, and S. P. Papadopoulos, Seismic performance of industrial pressure vessels: parametric investigations of simplified modeling approaches for vulnerability assessment. 5th International Conference on Computational Methods in Structural Dynamics and Earthquake Engineering (COMPDYN 2015) (2015) 2021–2037, https://doi.org/10.7712/120115.3520.944

[15] G. W. Housner, The dynamic behavior of water tanks. Bulletin of the Seismological Society of America 53 (2) (1963) 381–387, https://doi.org/10.1785/BSSA0530020381

[16] P. K. Malhotra and A. S. Veletsos, Uplifting response of unanchored liquid-storage tanks. Journal of Structural Engineering 120 (12) (1994) 3525–3547, https://doi.org/10.1061/(asce)0733-9445(1994)120:12(3525)

[17] P. K. Malhotra, Earthquake induced sloshing in tanks with insufficient freeboard. Structural Engineering International 16 (3) (2006) 222–225, https://doi.org/10.2749/101686606778026466

[18] K. Bakalis, M. Fragiadakis, and D. Vamvatsikos, Surrogate Modeling for the Seismic Performance Assessment of Liquid Storage Tanks. Journal of Structural Engineering 143 (4) (2017) 04016199, https://doi.org/10.1061/(ASCE)ST.1943-541X.0001667

[19] O. S. Bursi, M. S. Reza, G. Abbiati, and F. Paolacci, Performance-based earthquake evaluation of a full-scale petrochemical piping system. Journal of Loss Prevention in the Process Industries 33 (2015) 10–22, https://doi.org/10.1016/j.jlp.2014.11.004

[20] L. Di Sarno and G. Karagiannakis, On the seismic fragility of pipe rack—piping systems considering soil–structure interaction. Bulletin of Earthquake Engineering 18 (6) (2020) 2723–2757, https://doi.org/10.1007/s10518-020-00797-0

[21] N. D. Karaferis, A. K. Kazantzi, V. E. Melissianos, K. Bakalis, and D. Vamvatsikos, Seismic fragility assessment of high-rise stacks in oil refineries. Bulletin of Earthquake Engineering 20 (12) (2022) 6877–6900, https://doi.org/10.1007/s10518-022-01472-2

[22] A. K. Kazantzi, N. D. Karaferis, V. E. Melissianos, K. Bakalis, and D. Vamvatsikos, Seismic fragility assessment of building-type structures in oil refineries. Bulletin of Earthquake Engineering 20 (12) (2022) 6853–6876, https://doi.org/10.1007/s10518-022-01476-y

[23] G. Karagiannakis, L. Di Sarno, A. Necci, and E. Krausmann, Seismic risk assessment of supporting structures and process piping for accident prevention in chemical facilities. International Journal of Disaster Risk Reduction 69 (2022) 102748, https://doi.org/10.1016/j.ijdrr.2021.102748

[24] C. Grajales-Ortiz, V. E. Melissianos, K. Bakalis, M. Kohrangi, P. Bazzurro, and D. Vamvatsikos. Seismic damage assessment of a crude oil hydrodesulphurisation unit. Part II: hazard-consistent fragility assessment. International Journal of Disaster Risk Reduction (under review) (2025).

[25] J. Ancheyta, Modeling and Simulation of Catalytic Reactors for Petroleum Refining. Wiley, Hoboken, NJ (2011), https://doi.org/10.1002/9780470933565

[26] European Parliament, Directive 2009/30/EC of the European Parliament and of the Council of 23 April 2009 amending Directive 98/70/EC as regards the specification of petrol, diesel and gas-oil and introducing a mechanism to monitor and reduce greenhouse gas emissions and amending Council Directive 1999/32/EC as regards the specification of fuel used by inland waterway vessels and repealing Directive 93/12/EEC, Brussels (2009), https://eur-lex.europa.eu/legal-content/EN/TXT/?uri=celex%3A32009L0030

[27] F. McKenna, OpenSees: A framework for earthquake engineering simulation. Computing in Science and Engineering 13 (4) (2011) 58–66, https://doi.org/10.1109/MCSE.2011.66

[28] ASME, ASME Boiler and Pressure Vessel Code (BPVC). Section VIII – Rules for Construction of Pressure Vessels. American Society of Mechanical Engineers, New York, NY (2023).

[29] API, Centrifugal Pumps for Petroleum, Petrochemical, and Natural Gas Industries, API Standard 610, 12th edition, American Petroleum Institute, Washington, DC (2021).

[30] API, Shell-and-Tube Heat Exchangers for General Refinery Services, API Standard 660, 10th edition, American Petroleum Institute, Washington, DC (2020).

[31] N. D. Karaferis, V. E. Melissianos, and D. Vamvatsikos, Mechanical modeling, seismic fragility, and correlation issues for groups of spherical pressure vessels. Acta Mechanica 235 (3) (2024) 1563–1582, https://doi.org/10.1007/s00707-023-03670-8

[32] CEN, Eurocode 8: design of structures for earthquake resistance. Part 1: General rules, seismic actions and rules for buildings. EN1998-1, European Committee for Standardization, Brussels (2004), https://eurocodes.jrc.ec.europa.eu/EN-Eurocodes/eurocode-8-design-structures-earthquake-resistance

[33] ASCE/SEI, Minimum Design Loads and Associated Criteria for Buildings and Other Structures. American Society of Civil Engineers, Reston, VA (2017), https://doi.org/10.1061/9780784414248

[34] C. Thomas, Process Technology Equipment and Systems (Third edition). Cengage Learning, Inc, Boston, MA (2014), ISBN: 1435488245

[35] A. Chaibakhsh, N. Ensansefat, A. Jamali, R. Kouhikamali, and H. Najafi, Crude oil direct fired furnace model. Applied Thermal Engineering 83 (2015) 57–70, https://doi.org/10.1016/j.applthermaleng.2015.02.074

[36] A. Braconi, M. Finetto, H. Degee, N. Hausoul, et al., Optimising the seismic performance of steel and steel-concrete structures by standardising material quality control (OPUS). Publications Office of the European Union, Luxembourg (2013), https://doi.org/10.2777/79330

[37] S. Xu, Y. Wang, and X. Feng, Plant layout optimization with pipe rack and frames. Chemical Engineering Transactions 81 (2020) 265-270, https://doi.org/10.3303/CET2081045

[38] S. A. Karamanos, D. Tsouvalas, and A. M. Gresnigt, Ultimate bending capacity and buckling of pressurized 90 deg steel elbows. Journal of Pressure Vessel Technology 128 (3) (2006) 348–356, https://doi.org/10.1115/1.2217967

[39] L. Zeng, L. G. Jansson, and Y. Venev, On Pipe Elbow Elements in ABAQUS and Benchmark Tests. Volume 3: Design and Analysis. ASME 2014 Pressure Vessels and Piping Conference (2014) V003T03A036, https://doi.org/10.1115/PVP2014-28920

[40] F. Paolacci, M. S. Reza, and O. S. Bursi, Seismic design criteria of refinery piping systems. 3rd International Conference on Computational Methods in Structural Dynamics and Earthquake Engineering (COMPDYN 2011), Corfu (2011), https://eccomas.org/wp-content/uploads/2019/10/TC-PROCEEDINGS-2011-COMPDYN.pdf

[41] S. A. Karamanos, Mechanical behavior of steel pipe bends: An overview. Journal of Pressure Vessel Technology 138 (4) (2016) 041203, https://doi.org/10.1115/1.4031940

[42] U. Zahid, S. Z. Khan, M. A. Khan, H. J. Bukhari, I. Ahmed, and K. A. Khan, A methodology for flexibility analysis of process piping. Institution of Mechanical Engineers, Part E: Journal of Process Mechanical Engineering 232 (6) (2018) 751–761, https://doi.org/10.1177/0954408917738963

[43] CEN, Metallic Industrial Piping. Part 3: Design and Calculation. EN 13480-3:2017, European Committee for Standardisation, Brussels (2017).

[44] ASME, ASME B31.3. Process Piping, ASME Code for Pressure Piping, B31. American Society of Mechanical Engineers, New York, NY (2022), https://www.asme.org/codes-standards/find-codes-standards/b31-3-process-piping

[45] K. Thomas, Stiffening effects on thin-walled piping elbows of adjacent piping and nozzle constraints. Journal of Pressure Vessel Technology 104 (3) (1982) 180–187, https://doi.org/10.1115/1.3264201

[46] M. Martinez, J. Bracamonte, and M. Gonzalez, Bend flexibility factors of piping elbows and piping elbows with trunnion attachments using the boundary element method. Volume 2: Computer Applications/Technology and Bolted Joints, ASME 2009 Pressure Vessels and Piping Conference (2009) 25–32, https://doi.org/10.1115/PVP2009-77799

[47] M. Haji Mohammad Karim, In-plane flexibility factor of 90 degree long radius elbows with large diameter. Volume 2: Computer Technology and Bolted Joints; Design and Analysis. ASME 2021 Pressure Vessels and Piping Conference (2021) V002T03A007, https://doi.org/10.1115/PVP2021-61533

[48] W. Ramberg and W. R. Osgood, Description of stress-strain curves by three parameters. Technical Note No. 902, National Advisory Committee for Aeronautics, Washington DC (1943), https://ntrs.nasa.gov/api/citations/19930081614/downloads/19930081614.pdf

[49] G. P. Kouretzis, D. K. Karamitros, and S. W. Sloan, Analysis of buried pipelines subjected to ground surface settlement and heave. Canadian Geotechnical Journal 52 (8) (2015) 1058–1071, https://doi.org/10.1139/cgj-2014-0332